

**ATTENUATION OF SCALAR FLUXES
MEASURED WITH HORIZONTALLY-DISPLACED SENSORS**

T.W. Horst

National Center for Atmospheric Research, Boulder, CO

1. INTRODUCTION

Turbulent scalar fluxes are determined by correlating vertical velocity measurements, commonly made on towers with a sonic anemometer, with scalar density measurements made with an appropriate fast response sensor, e.g. an open-path optical-absorption hygrometer in the case of water vapor fluxes. In order to avoid flow distortion errors in the velocity measurements, in-situ scalar sensors must be displaced from the measurement volume of the sonic anemometer. Unfortunately this causes a decorrelation of the velocity and scalar density measurements and a reduction in the measured flux. As noted by Kristensen et al. (1997), it is expected that the attenuation of the measured flux will be “an increasing function of the ratio of the sensor displacement and the scale of the turbulence”. In the surface layer, the integral scale of the vertical velocity component increases with height, and therefore the flux attenuation will increase with the ratio of sensor displacement to the measurement height. The measured flux can be corrected simply by dividing it by the estimated fractional attenuation of the measured flux.

Two recent papers examined this issue with extensive data sets that used temperature as the measured scalar variable, with the assumption that by scalar similarity the observed attenuation in the heat flux can be applied equally as well to other scalar fluxes (Hill, 1989). Lee and Black (1994, hereafter LB) collected data during neutral to unstable stratification using two horizontal, orthogonal, linear arrays of five thermocouples each, combined with a vertical-axis sonic anemometer and thermocouple co-located at the intersection of the two arrays. They computed the displaced scalar flux $F(r_x, r_y)$ by eddy covariance using thermocouples displaced from the sonic anemometer by r/z ranging from 0.07 to 1.23, as well as the scalar flux with co-located sensors, $F_o \equiv F(0, 0)$. Here (r_x, r_y) are the streamwise and crosswind sensor displacements, $r^2 \equiv r_x^2 + r_y^2$, and z is measurement height.

LB found that their observed fluxes were in good agreement with their formula

$$F(r_x, r_y) = F_o \exp[-\alpha(\theta)\phi_h\phi_\epsilon^{1/3}(r/z)^{4/3}] \quad (1)$$

Here ϕ_h and ϕ_ϵ are the usual dimensionless micrometeorological functions that describe the dependence of the vertical potential temperature gradient and turbulent dissipation on atmospheric stability, z/L , where L is the Obukhov length. LB derived the functional dependence of $F(r_x, r_y)$ on z/L and $(r/z)^{4/3}$ with the assumption of inertial range scaling, that is, the sensor displacement was assumed to be small enough to be comparable to inertial-range turbulence scales.

The dependence of Eq. (1) on wind direction is

$$\alpha(\theta) = 1.18(\cos^2\theta + 2.4\sin^2\theta)^{2/3} \quad , \quad (2)$$

where θ is the wind direction with respect to the direction of the sensor displacement. LB based the functional dependence on wind direction on the assumption that the turbulent eddies have an elliptical shape in the horizontal, while the numerical coefficients in (2) were found from an empirical fit to their observations. Eq. (2) implies that the decorrelation of vertical velocity and temperature is more than twice as sensitive to crosswind displacement ($\theta = \pi/2$) than to streamwise displacement ($\theta = 0$).

Kristensen et al. (1997, hereafter KMOW) measured scalar flux attenuation caused by both horizontal and vertical displacements. The fluxes with horizontal displacements were measured for three values of r/z , 0.083, 0.17, and 0.25, and 90% of their data fall within the ranges $-2 < z/L < 0$ and $|90^\circ - \theta| < 45^\circ$ (equivalently, $r_y > r_x$). Within these ranges, KMOW did not observe “any systematic variation” of $F(r_x, r_y)/F_o$ with wind direction and “no large variation” with stability. Then, with the assumption that $F(r_x, r_y)/F_o$ is independent of wind direction, they find

$$F(r_x, r_y) = \int_{-\infty}^{\infty} C_{owc}(k) \cos(kr) dk \quad , \quad (3)$$

where k is wavenumber and $C_{o_{wc}}(k)$ is the cospectrum for co-located measurements of vertical velocity and scalar density. KMOW model the cospectrum by fitting observations to

$$Co(k) = \frac{A(\mu)F_o}{k_m[1 + 0.75(k/k_m)^{2\mu}]^{7/6\mu}} \quad , \quad (4)$$

where $k_m = 2\pi n_m/z$ is the wavenumber at the peak of the wavenumber-multiplied cospectrum $kCo(k)$. Using $\mu = 0.23$ and $n_m = 0.07$, they find that the predictions of Eqs. (3–4) provide a reasonable match to their data. Since their data and the predictions of Eqs. (3–4) both fall within the range predicted by Eqs. (1–2) for $\theta = 60^\circ$ and $-2 < z/L < 0$, KMOW also note that “our measurement and theory are not in direct contradiction with Lee and Black”.

Despite the valuable field observations and the theoretical advances found in the papers by Lee and Black (1994) and Kristensen et al. (1997), there remain contradictions between these two papers and the range of the available data is limited. LB observe a dependence of $F(r_x, r_y)/F_o$ on $(r/z)^{4/3}$ which theoretically should only apply for very small sensor displacements. They also find a dependence on stability and wind direction which apparently is not observed in the KMOW data. Further, neither paper contains significant amounts of data for horizontal displacements in stable stratification. The present paper attempts to shed some light on these issues using a recent data set from the Horizontal Array Turbulence Study (HATS) field project.

2. Theoretical Analysis

The cross covariance measured with a spatial sensor displacement $\mathbf{r} = (r_x, r_y, r_z)$ is equal to

$$\overline{w'(\mathbf{x})c'(\mathbf{x} + \mathbf{r})} = \iiint_{-\infty}^{\infty} e^{i\mathbf{k}\cdot\mathbf{r}} \Phi_{wc}(\mathbf{k}) d^3k \quad (5)$$

$$= \int_{-\infty}^{\infty} e^{ik_1 r} Cr_{wc}(k_1) dk_1 \quad (6)$$

(e.g. Lumley and Panofsky, 1964, p. 26ff). Here $\mathbf{k} = (k_x, k_y, k_z)$, $\Phi_{wc}(\mathbf{k})$ is the three-dimensional cross spectrum between vertical velocity and scalar density at the same location, k_1 is the wavenumber parallel to the spatial displacement, i.e. $\mathbf{k}\cdot\mathbf{r} \equiv k_1 r$, and $Cr_{wc}(k_1)$ is the one-dimensional cross spectrum along k_1 ,

$$Cr_{wc}(k_1) \equiv \iint_{-\infty}^{\infty} \Phi_{wc}(\mathbf{k}) dk_2 dk_3 \quad . \quad (7)$$

The cross spectrum can be separated into real and imaginary parts,

$$Cr_{wc}(k_1) = Co_{wc}(k_1) - iQ_{wc}(k_1) \quad , \quad (8)$$

where $Co_{wc}(k_1)$ and $Q_{wc}(k_1)$ are the one-dimensional cospectrum and quadrature spectrum, respectively. For co-located variables, it can be assumed that $Q_{wc} \ll Co_{wc}$, and therefore,

$$F(\mathbf{r}) = \int_{-\infty}^{\infty} Co_{wc}(k_1) \cos(k_1 r) dk_1 \quad . \quad (9)$$

If \mathbf{r} lies in the horizontal plane and it is assumed as in KMOW that $Co(k_1)$ is circularly symmetric, then Eq. (3) follows from (9). In the more general case, Eq. (9) is most useful when \mathbf{r} is in the streamwise direction, because with the assumption of Taylor’s hypothesis we can estimate the form of $Co(k_x)$ from time series data.

If it is assumed that the KMOW one-dimensional cospectrum, Eq. (4), applies in any direction, then Eq. (9) can be written as

$$F(\mathbf{r}) = A(\mu)F_o \int_{-\infty}^{\infty} \frac{\cos(k_{1m} r k')}{[1 + 0.75k'^{2\mu}]^{7/6\mu}} dk' \quad , \quad (10)$$

where $k' = k_1/k_{1m}$ and k_{1m} is the wavenumber at the maximum of the wavenumber-multiplied cospectrum along the coordinate parallel to \mathbf{r} . Thus we obtain the useful result that $F(\mathbf{r}) = f(k_{1m} r, \mu)$. The independent variable $k_{1m} r$ can be written either in the form $2\pi r/\lambda_{1m}$, where λ_{1m} is the wavelength of the cospectral maximum parallel to the sensor displacement, or in the form $2\pi n_{1m} r/z$, where $n_{1m} = z/\lambda_{1m}$ is a dimensionless function of stability (Kaimal et al., 1972). Thus the independent variable $k_{1m} r$ contains explicitly the expected dependence on r/λ_{1m} or r/z noted in the Introduction, as well as an implicit dependence on stability and wind direction. Using the HATS data, to be described in the next section, we find that the KMOW cospectrum provides a reasonable fit to streamwise cospectra with $\mu \simeq 1/4$ for unstable stratification and $\mu \simeq 1/2$ for stable stratification. Using the KMOW cospectrum, we can then estimate flux attenuation by numerically integrating (10) and investigating its dependence on $k_{1m} r$ and stability.

We first examine the result of LB that the flux attenuation depends on $(r/z)^{4/3}$. Assuming

a form of $Co(k)$ appropriate for inertial turbulence, KMOW integrate (3) and obtain a result equivalent to that of LB,

$$F(r) \approx F_o [1 - (9/4)B\Gamma(2/3)(r/z)^{4/3}] \quad , \quad (11)$$

where B is a stability-dependent parameter. Figure 1 shows the quantity $1 - F(r)/F_o$ as a function of $k_m r$, obtained by numerical integration of KMOW stable and unstable cospectra and the Kansas (streamwise) neutral cospectrum of Kaimal et al. (1972). Also shown are asymptotes to these curves corresponding to the inertial range result, $1 - F(r)/F_o \sim (r/z)^{4/3}$. It can be seen that the flux attenuation for realistic cospectra is dependent on $(r/z)^{4/3}$ only for sensor displacements so small that $F(r)/F_o \geq 0.99$.

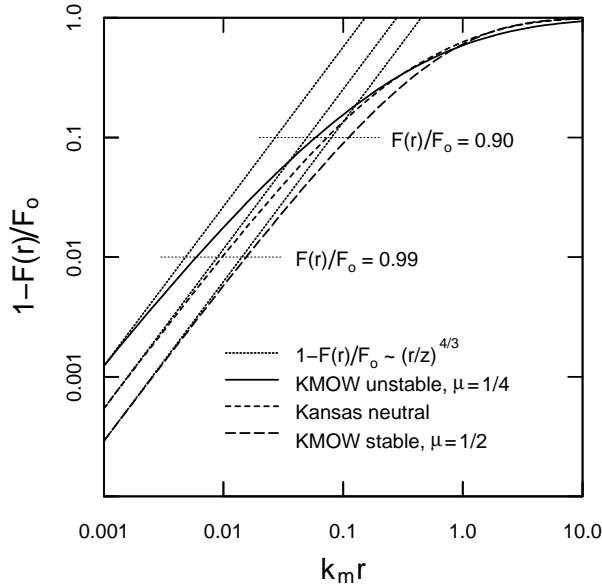


Figure 1. Test of Eq. (1), $F(r)/F_o \sim (r/z)^{4/3}$.

Alternately, an analytical formula for the flux attenuation can be obtained by assuming a cospectrum of the form,

$$Co(k) = \frac{2}{\pi k_m [1 + (k/k_m)^2]} \quad . \quad (12)$$

Although this cospectrum departs from the theoretical inertial-range slope of $-7/3$ used in the KMOW cospectrum, Horst (1997) finds that it provides a close match to the Kansas stable cospectrum of Kaimal et al. (1972). With this cospectrum, Eq. (9) can be integrated analytically to obtain

$$F(r) = F_o \exp(-k_m r) \quad . \quad (13)$$

Figure 2 shows $F(r)/F_o$ as a function of $k_m r$ for the same cospectra used in Figure 1 and compares them to the formula of Eq. (13). This formula departs significantly from the flux attenuation estimated for neutral and unstable stratification, but for stable stratification it provides a very good match for flux attenuation as large as 50%.

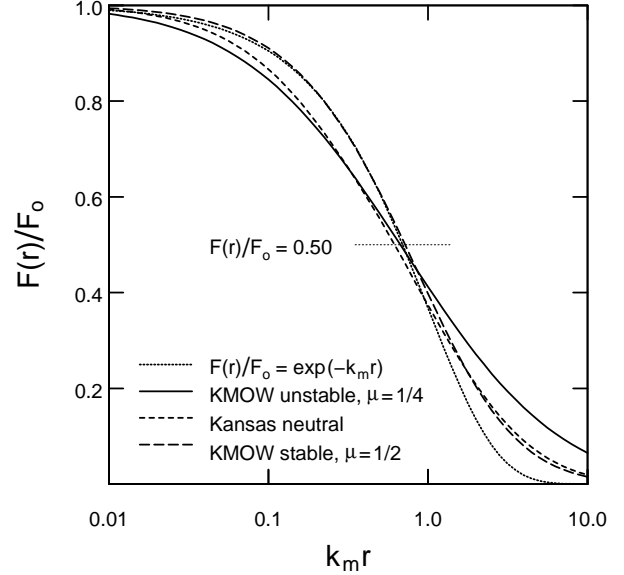


Figure 2. Test of Eq. (13), $F(r)/F_o = \exp(-k_m r)$.

3. HATS Field Observations

The Horizontal Array Turbulence Study (Horst et al., 2004) collected data from two parallel, horizontal arrays of sonic anemometers oriented in the climatological crosswind direction. The two arrays, labeled s and d , were composed of 5 and 9 equally-spaced sonic anemometers respectively, with one array located directly above the other as shown in Figure 3. Table 1 lists the

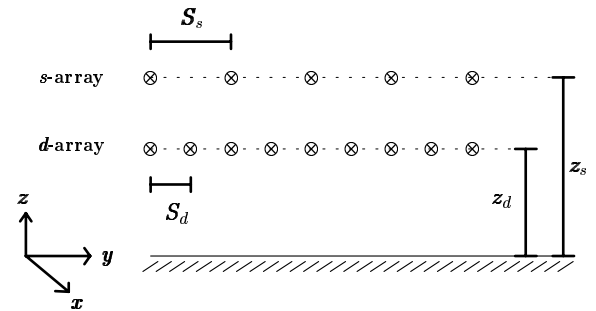


Figure 3. Schematic of the two HATS horizontal sonic arrays at heights $\{z_d, z_s\}$ agl and with crosswind sonic separations $\{S_s, S_d\}$.

heights and sonic spacings of the four HATS configurations. An aerodynamic displacement height h_d of 32 cm and a surface roughness length of 2 cm were calculated from near-neutral wind profiles measured at the site. The range of $r/(z_{agl} - h_d)$ for HATS is 0.13–8.56. Two sonics were also mounted at heights z_s and z_d on each of two additional towers, which were located along a line normal to the crosswind sonic arrays for the purpose of measuring the turbulence advection velocity. The following results were calculated from 49 stationary, 25–60 minute periods which were selected to cover a wide range of stability from each of the four sonic configurations.

Table 1. HATS Transverse Array Dimensions (m)

Configuration	z_d (m agl)	S_d (m)	z_s (m agl)	S_s (m)
1	3.45	3.35	6.90	6.70
2	4.33	2.17	8.66	4.33
3	8.66	2.17	4.33	1.08
4	4.15	0.50	5.15	0.63

4. Streamwise Sensor Displacements

In order to investigate flux attenuation caused by spatial sensor displacement, virtual temperature fluxes were calculated by correlating sonic anemometer measurements of vertical velocity w

and temperature derived from the speed of sound, tc . The fluxes for streamwise sensor displacements, $F(r_x)$, were estimated by assuming Taylor’s hypothesis and lagging the time series for one variable by $\delta t = r_x/U_a$ with respect to the other variable for each sonic. Here U_a is a turbulence advection velocity equal to 1.06 times the mean wind speed. U_a was estimated as $d/\Delta t$, where d is the streamwise separation of the HATS advection towers and Δt is the time lag required for maximum correlation between w' and tc' measured at the two towers. Positive r_x corresponds to the scalar measurement downstream of the vertical velocity measurement. The flux attenuation was determined for each analysis period by dividing $F(r_x)$ by the co-located flux F_o for each sonic and then averaging the flux ratios over all sonics at each height.

Figures 4a and 4b show flux attenuation for unstable and stable stratification, respectively. Here k_{mx} were determined by fitting the KMOW cospectrum, Eq. (4), to the (co-located) HATS streamwise cospectra using $k_x = 2\pi f/U_a$, where f is frequency. The data points are the medians of the measured flux attenuation within each $k_{mx}r_x$ interval. The vertical lines with each point denote the quantiles of its corresponding data distribution for 15% and 85% cumulative probability, which are equivalent to \pm one standard deviation for a normal distribution.

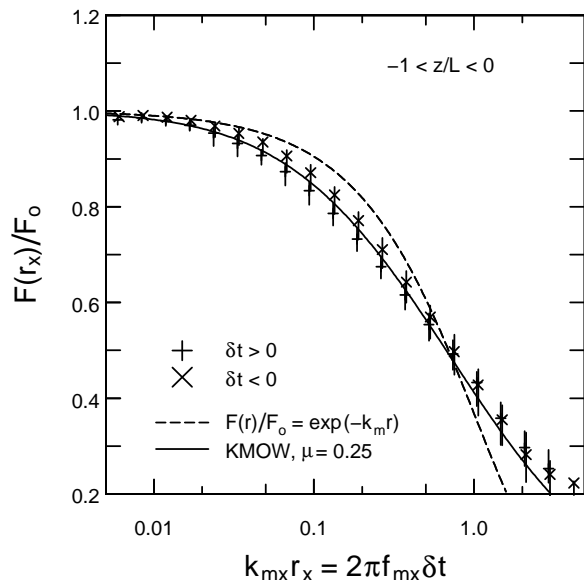


Figure 4a. Flux attenuation for streamwise sensor displacements and unstable stratification.

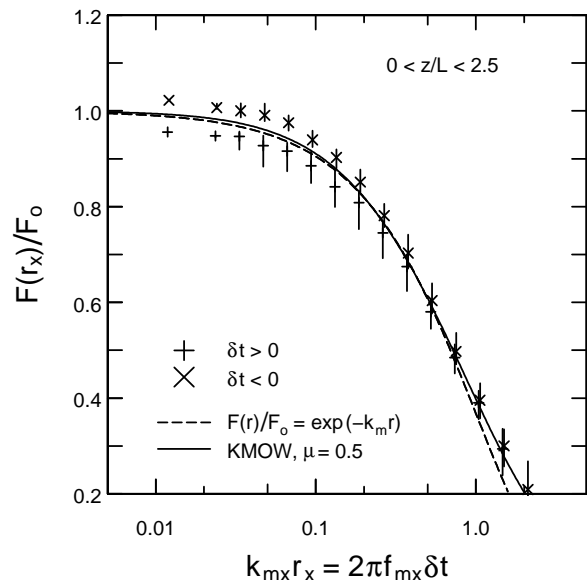


Figure 4b. Flux attenuation for streamwise sensor displacements and stable stratification.

Points are shown separately for positive and negative streamwise sensor displacements. Flux attenuation with the scalar sensor upwind of the sonic ($\delta t < 0$) is systematically less than that for the opposite configuration, although the difference between the two displacements is often less than the total range of the data for each $k_{mx}r_x$ interval. The noticeable asymmetry for positive and negative displacements is present for all stabilities and is thought to be a consequence of the asymmetric plume structure commonly found in the surface layer for temperature as well as other scalars. These plumes are characterized by sharp scalar fronts at their leading edge, and this structure causes the scalar flux to decay more rapidly for positive sensor displacements than for negative displacements.

As suggested by the empirical cospectral formulas used in Figure 2, $F(r_x)/F_o$ as a function of $k_{mx}r_x$ is noticeably different for stable and unstable stratification, but with little systematic dependence on stability within either stability class. Curves are shown for both the exponential attenuation model, Eq. (13), and for the numerical integration of the KMOW cospectrum, Eq. (10). The mean of the HATS data for positive and negative r_x is matched quite closely by Eq. (10) with $\mu = 0.25$ for unstable stratification and $\mu = 0.5$ for stable stratification, with the exception of attenuation greater than 50% for unstable stratification. The stably stratified HATS data is

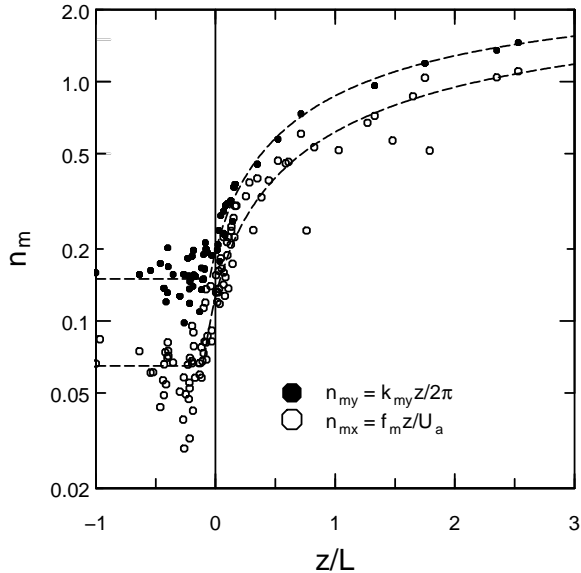


Figure 5. Dimensionless frequency at the maxima of the streamwise and crosswind cospectra.

also matched quite well by the exponential model for flux attenuation up to 50%. As will be shown next, k_{mx} varies over a wide range for stable stratification, and thus without k_{mx} in the abscissa, the data would not collapse as closely to a single relation as seen here.

Figure 5 shows $n_{mx} = f_m z / U_a$ as a function of z/L for the HATS data. For unstable stratification, n_{mx} is roughly constant, but exhibits a great deal of scatter, which is associated with large case-to-case variations in the low wavenumber portion of the scalar flux cospectrum. However for near-neutral and stable stratification, n_m increases systematically, changing by a factor greater than 10. This overall behavior is identical to that found by Kaimal and Finnigan (1994) with previous data sets. The HATS data are fit by the empirical formula,

$$n_{mx} = \begin{cases} 0.066, & z/L \leq -0.1; \\ 2.18 - 2.114/(1.015 + 0.15z/L)^2, & z/L > -0.1. \end{cases} \quad (14)$$

5. Crosswind Sensor Displacements

The fluxes for crosswind sensor displacements, $F(r_y)$, were calculated after projecting the HATS data from each of the two arrays onto lines normal to the mean wind direction by lagging the data from each sonic by $\delta t = jS \sin \Theta / U$. Here Θ is the mean wind direction at each height relative to the array normal ($\Theta = 0$ for wind normal to the array) and j is the integer position of each sonic in the array relative to the central sonic, e.g. for the 9-sonic d array, $-4 < j < 4$. Because of the need to project the data onto the crosswind direction, data for crosswind sensor displacements were limited to wind directions within $\pm 33^\circ$ of the array normal. The flux attenuation for each crosswind spatial displacement was determined by averaging together all possible sonic combinations with a given separation. Figure 6 shows the flux attenuation as a function of $k_{my}r_y$. For crosswind displacements, k_{my} was estimated for each data period and height by a fit of the exponential model to the flux attenuation data. As can be seen, the data correspond reasonably well to the exponential attenuation model across the entire range of stability, particularly for unstable stratification.

Figure 5 also shows n_{my} as a function of z/L . The dependence of n_{my} on stability is very similar

to that for n_{mx} , but n_{mx} is systematically smaller than n_{my} . This occurs because vertical shear elongates the eddies in the streamwise direction, placing the peak of the streamwise cospectrum at lower wavenumbers. As a consequence, the scalar flux decays more slowly in the streamwise direction than in the crosswind direction. For unstable stratification, the difference in decay rates is greater than a factor of 2, while for stable stratification the difference is only about 15%. The HATS data are fit by the empirical formula,

$$n_{my} = \begin{cases} 0.15, & z/L \leq -0.05; \\ 2.43 - 2.28/(1.01 + 0.2z/L)^2, & z/L > -0.05. \end{cases} \quad (15)$$

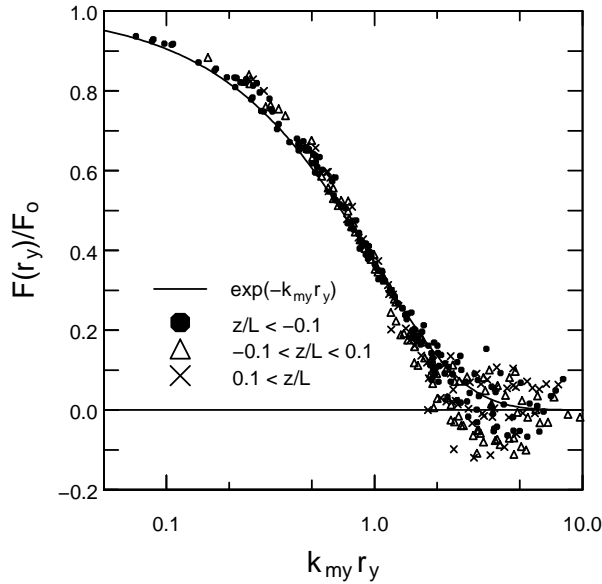


Figure 6. Flux attenuation for crosswind sensor displacements.

6. Dependence on Wind Direction

Although we have separated the flux attenuation analysis into crosswind and streamwise sensor displacements, the general case will be composed of some combination of the two displacements, $\mathbf{r} = (r_x, r_y)$. If the horizontal cross section of an eddy is assumed to be elliptical, as suggested by LB, then

$$\frac{1}{\lambda_m^2(\theta)} = \frac{\cos^2 \theta}{\lambda_{mx}^2} + \frac{\sin^2 \theta}{\lambda_{my}^2}, \quad (16)$$

or equivalently,

$$k_m(\theta) = (k_{mx}^2 \cos^2 \theta + k_{my}^2 \sin^2 \theta)^{1/2}. \quad (17)$$

LB's dependence on wind direction, Eq. (2), is similar to Eq. (17) with an implied value of $k_{my}/k_{mx} = 2.4^{2/3} = 1.8$. Correspondingly, Eqs. (14–15) for the HATS data give $1.5 \leq k_{my}/k_{mx} \leq 2.3$ for neutral to unstable stratification, the range of LB's data.

Then, since $\cos \theta = r_x/r$,

$$k_m r = (k_{mx}^2 r_x^2 + k_{my}^2 r_y^2)^{1/2}. \quad (18)$$

If it is further assumed that

$$A_x \equiv F(r_x)/F_o = \exp(-k_{mx} r_x) \quad (19)$$

$$A_y \equiv F(r_y)/F_o = \exp(-k_{my} r_y) \quad (20)$$

$$F(r_x, r_y)/F_o = \exp(-k_m r) \quad , \quad (21)$$

then

$$F(r_x, r_y) = F_o \exp \left[- (\ln^2 A_x + \ln^2 A_y)^{1/2} \right]. \quad (22)$$

Note that with the exception of streamwise displacements combined with unstable stratification, Eqs. (19–20) have been found to be good approximations to the HATS data.

The validity of Eq. (22) can be tested directly with the HATS data using observations of A_x , A_y , and $F(r_x, r_y)/F_o$. Figure 7 shows $F(r_x, r_y)/F_o$ for a moderately unstable case, $z/L = -0.4$, as a function of θ , the wind direction relative to the sensor displacement. The data are plotted separately for each of the eight crosswind sensor displacements available in the d-array of the fourth HATS sonic configuration, with r_y/z ranging from 0.13 to 1.04. The discrete data points are the observed values of $F(r_x, r_y)/F_o$, with each point corresponding to a streamwise sensor displacement $nU_a \delta t$ where δt is the sample spacing of the time series data, 0.05 sec. The lines on the plot are the predictions of Eq. (22) using the corresponding observed values of A_x and A_y .

As can be seen, Eq. (22) is identically valid for $\theta = 0^\circ$, 90° and 180° and, for flux attenuation less than about 40%, is a very good approximation for all wind directions. The error increases with increasing sensor displacement, and the maximum errors occur roughly in the two ranges $15^\circ < \theta < 45^\circ$ and $135^\circ < \theta < 165^\circ$. The maximum errors are shifted to wind directions less than 45° and greater than 135° (or $r_x > r_y$) because the

flux attenuation for a given sensor displacement is greater in the crosswind direction than in the streamwise direction. Similar results are found for all stabilities, although the errors in Eq. (22) are somewhat smaller for near-neutral and stable stratification, presumably because Eq. (19) is a better approximation for those conditions.

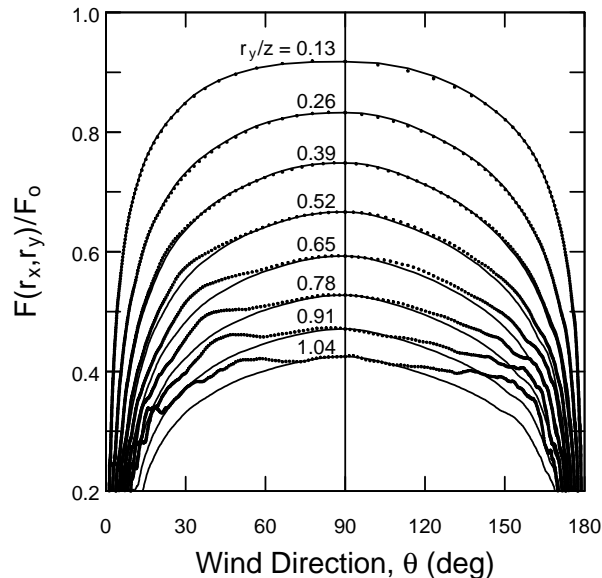


Figure 7. Test of Eq. (22) for $F(r_x, r_y)/F_o$ as a function of wind direction relative to the sensor displacement; $r_x/z = 0.028n$, $z/L = -0.4$.

The comparison shown in Figure 7 does not explicitly test the individual models for $F(r_x)/F_o$ and $F(r_y)/F_o$. This is done in Figure 8 where we again use Eq. (22) to combine streamwise and crosswind displacements, but estimate $F(r_x)$ with Eqs. (10) and (14), using $\mu = 0.25$ for unstable and 0.5 for stable stratification, and estimate $F(r_y)$ with Eqs. (20) and (15). Figure 8 is based on 9 unstable and 5 stable cases from the third and fourth HATS configurations, which have the smallest values of r_y/z and thus correspond to sensor displacements likely to be used for flux measurements. The data points correspond to the median values of the model estimates within each interval of the measured values, and the vertical bars again denote the 15% and 85% quantiles of the estimated-flux-attenuation distribution within each interval. The rms deviation from the 1:1 line is on the order of 5%, and a linear fit to the model estimates is $y = 0.98x + 0.01$.

7. Conclusions and Discussion

Scalar flux attenuation for horizontal displacements of the scalar and vertical velocity sensors is a function of the magnitude and direction of the displacement and of the dependence of the $\overline{w'c'}$ cospectrum on wavenumber. We find that flux attenuation for streamwise sensor displacements can be estimated quite well by the integral of the KMOW cospectral formula, Eq. (10), using stability-dependent values for μ , a parameter describing the shape of the cospectrum, and k_{mx} , the wavenumber at the peak of the cospectrum. The attenuation due to crosswind sensor displacement (as well as streamwise sensor displacement in stable stratification) can be estimated comparatively simply with the exponential model of Eq. (20). Assumption of the exponential model for both streamwise and crosswind attenuation permits a very simple expression, Eq. (22), for the flux attenuation due to a horizontal displacement composed of both streamwise and crosswind displacements. That expression is found to provide good estimates for flux attenuation as large as 40% or more.

Our estimates of flux attenuation for streamwise sensor displacements are based on the assumption of Taylor's hypothesis with a turbulence advection velocity equal to 1.06 times the wind speed. Thus if the investigator has retained the turbulence time series data, numerical integration of Eq. (10) and specification of a turbulence advection velocity can be avoided by similarly

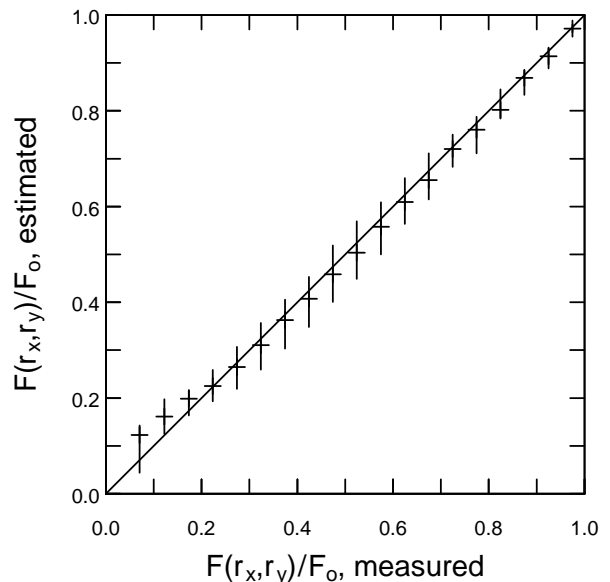


Figure 8. Test of HATS model for $F(r_x, r_y)/F_o$.

using Taylor’s hypothesis to simply lag or delay the data from the upstream sensor by the time difference required to maximize the correlation between w' and c' . Then from Eqs. (20) and (22), correction for attenuation due to any additional crosswind displacement is simply

$$F(0, r_y) = F(r_y) = F_o \exp(-k_{my} r_y). \quad (23)$$

These results were obtained with turbulence data measured within a horizontally-homogeneous surface-flux layer, that is, where the turbulence structure is found to depend only on height above the surface and on the surface fluxes of momentum and buoyancy as described by Monin–Obukhov similarity. The HATS flux attenuation formulas are not valid where the dependence on wavenumber of the scalar-flux cospectrum differs materially from that in the surface-flux layer, as is likely to be true for measurements in advective conditions, in complex terrain, over a wavy water surface, within a canopy, or within the roughness sublayer above the canopy. In these more complex situations, an empirical, in-situ technique suggested by Villalobos (1997) may be advantageous. This technique utilizes a temperature sensor placed near the scalar sensor to measure a displaced-sensor heat flux, which is then divided by the (co-located) sonic virtual heat flux to determine the flux attenuation in real time. Drawbacks of this technique include the required assumption of scalar similarity and the vanishing heat flux for neutral stratification.

Finally, we return to questions raised at the beginning of this paper. First, neither theoretical analysis nor comparison with the HATS data support the dependence of flux attenuation on $(r/z)^{4/3}$ for other than very small values of the ratio r/z . However, except for a difference in the exponent, the HATS data do support a model of wind direction dependence similar to that of LB’s Eq. (2).

The reason that KMOW find no dependence of flux attenuation on wind direction appears to be the limited range of their data, unstable stratification and $r/z \leq 0.25$. Within this range, the HATS flux attenuation model finds that $F(r_x)/F_o$ and $F(r_y = r_x)/F_o$ are within 2% of each other. While $k_{my} = 2.3 k_{mx}$ for unstable stratification (Figure 5), this difference is almost exactly compensated by the fact that, for the

range of the KMOW data ($k_m r \lesssim 0.1-0.2$), $F(r_x)/F_o$ decreases more rapidly as a function of $k_{mx} r_x$ (Figure 4a: KMOW, $\mu = 0.25$) than does $F(r_y)/F_o$ as a function of $k_{my} r_y$ (Figure 4a: $\exp(-k_m r)$).

Acknowledgements

The author is grateful to Leif Kristensen and Don Lenschow for helpful discussions of this research. The National Center for Atmospheric Research is funded by the National Science Foundation.

REFERENCES

- Hill, R., 1989, Implications of Monin–Obukhov similarity theory for scalar quantities. *J. Atmos. Sci.*, **46**, 2236–2244.
- Horst, T.W., 1997, A simple formula for attenuation of eddy fluxes measured with first-order-response scalar sensors. *Bound. Layer Meteorol.*, **82**, 219–233.
- Horst, T.W., J. Kleissl, D.H. Lenschow, C. Meneveau, C.–H. Moeng, M.B. Parlange, P.P. Sullivan, and J.C. Weil, 2004, HATS: Field observations to obtain spatially filtered turbulence fields from crosswind arrays of sonic anemometers in the atmospheric surface layer. *J. Atmos. Sci.*, **61**, 1566–1581.
- Kaimal, J.C., J.C. Wyngaard, Y. Izumi, and O.R. Cote, 1972, Spectral characteristics of surface-layer turbulence. *Quart. J. R. Met. Soc.*, **98**, 563–589.
- Kaimal, J.C., and J.J. Finnigan, 1994, *Atmospheric Boundary Layer Flows*, Oxford University Press, 189 pp.
- Kristensen, L., J. Mann, S.P. Oncley, and J.C. Wyngaard, 1997, How close is close enough when measuring scalar fluxes with displaced sensors? *J. Atmos. Ocean. Tech.*, **14**, 814–821.
- Lee, X., and T.A. Black, 1994, Relating eddy correlation sensible heat flux to horizontal sensor separation in the unstable atmospheric surface layer. *J. Geophys. Res.*, **99** (D9), 18545–18553.
- Lumley, J.L., and H.A. Panosky, 1964, *The Structure of Atmospheric Turbulence*, John Wiley & Sons, 239 pp.
- Villalobos, F.J., 1997, Correction of eddy covariance water vapor flux using additional measurements of temperature. *Ag. For. Meteorol.*, **88**, 77–83.